nature chemistry

Article

https://doi.org/10.1038/s41557-024-01648-0

Multi-stage and multi-colour liquid crystal reflections using a chiral triptycene photoswitchable dopant

Received: 17 August 2023

Accepted: 29 August 2024

Published online: 4 October 2024

Check for updates

Indu Bala[1], Joshua T. Plank[2], Brandon Balamut[1], Drake Henry[2], Alexander R. Lippert[2] & Ivan Aprahamian[1]

The photomodulation of the helical pitch of cholesteric liquid crystals results in dynamic and coloured canvases that can potentially be used in applications ranging from energy-efficient displays to colour filters, anti-counterfeiting tags and liquid crystal (LC) lasers. Here we report on the analysis of a series of photoswitchable chiral dopants that combine the large geometrical change and bistability of hydrazone switches with the efficient helical pitch induction of the chiral motif, triptycene. We elucidate the effects that conformational flexibility, dispersion forces and π–π interactions have on the chirality transfer ability of the dopant. We then use the irradiation time with visible light (442 nm) combined with a simple digital light processing microscope projection set-up to draw numerous stable multi-coloured images on an LC canvas, showcasing the fine control this dopant yields over the LC assembly.

The non-invasive and remote control over the properties of self-organized supramolecular architectures is a necessary step towards the fabrication of smart molecular materials and devices[1]. One approach to this end is to integrate molecular photoswitches into soft supramolecular materials as a means to reversibly manipulate their dynamic superstructures with the high spatiotemporal resolution of light[2]. A notable illustration of this concept is the use of photoswitchable chiral dopants in controlling the supramolecular helical self-assembly of liquid crystals (LCs)[3–7]. In such LC materials (known as cholesteric LCs (CLCs)) the periodic pitch length, P, controls the assembly's ability to selectively reflect light[8,9]. Adjusting the pitch of such assemblies (and hence reflected wavelength/colour) and locking them in at desired value(s) using photoswitchable dopants is one of the main challenges in the field[6,7,10–19]. Azobenzenes[20], which undergo large geometrical changes upon photoisomerization (that is, E/Z isomerization) and hence result in large helical twisting powers (β, that is, their ability to induce twisting in an achiral nematic LC) and/or change in β ($\Delta\beta$), have been extensively used in controlling the reflected colours from CLCs[6,7]. However, and in general, the relative fast thermal isomerization of the Z isomer of azobenzenes (that is, metastability) impedes the locking-in of the supramolecular helices and hence results in transient photophysical properties. While bistable diarylethene switches[21] have been used to address this issue[22,23], their limited shape change upon photoisomerization (that is, cycloaddition/reversion reaction) results in low β and $\Delta\beta$ values[23–29], with recently developed intrinsically chiral diarylethene photoswitches being an exception[30]. It is noteworthy that, unlike most reported dopants, the latter systems do not rely on binaphthyl-based chiral cores to obtain high β values, which is what most practitioners are limited to. Finally, there are no general guiding principles nor hypotheses that can be used in designing chiral dopants that have large β and $\Delta\beta$ values, and hence, practitioners rely on trial and error in their efforts[3,4].

Photochromic hydrazones[31–33], which are characterized by their bistability and significant geometric shape change upon photoisomerization (that is, Z/E isomerization), are primed to address these obstacles in the field. Nonetheless, our first attempt[34] in modulating LC properties using a hydrazone-based switchable dopant with isosorbide being the chiral motif, resulted in low β values (35 and 57 μm^{-1} for the Z-rich E-rich states, respectively). The latter limited the obtained reflectance wavelengths to the near infra-red (NIR) range. Nevertheless,

[1]Department of Chemistry, Dartmouth College, Hanover, NH, USA. [2]Department of Chemistry, Southern Methodist University, Dallas, TX, USA. e-mail: ivan.aprahamian@dartmouth.edu

https://doi.org/10.1038/s41557-024-01648-0

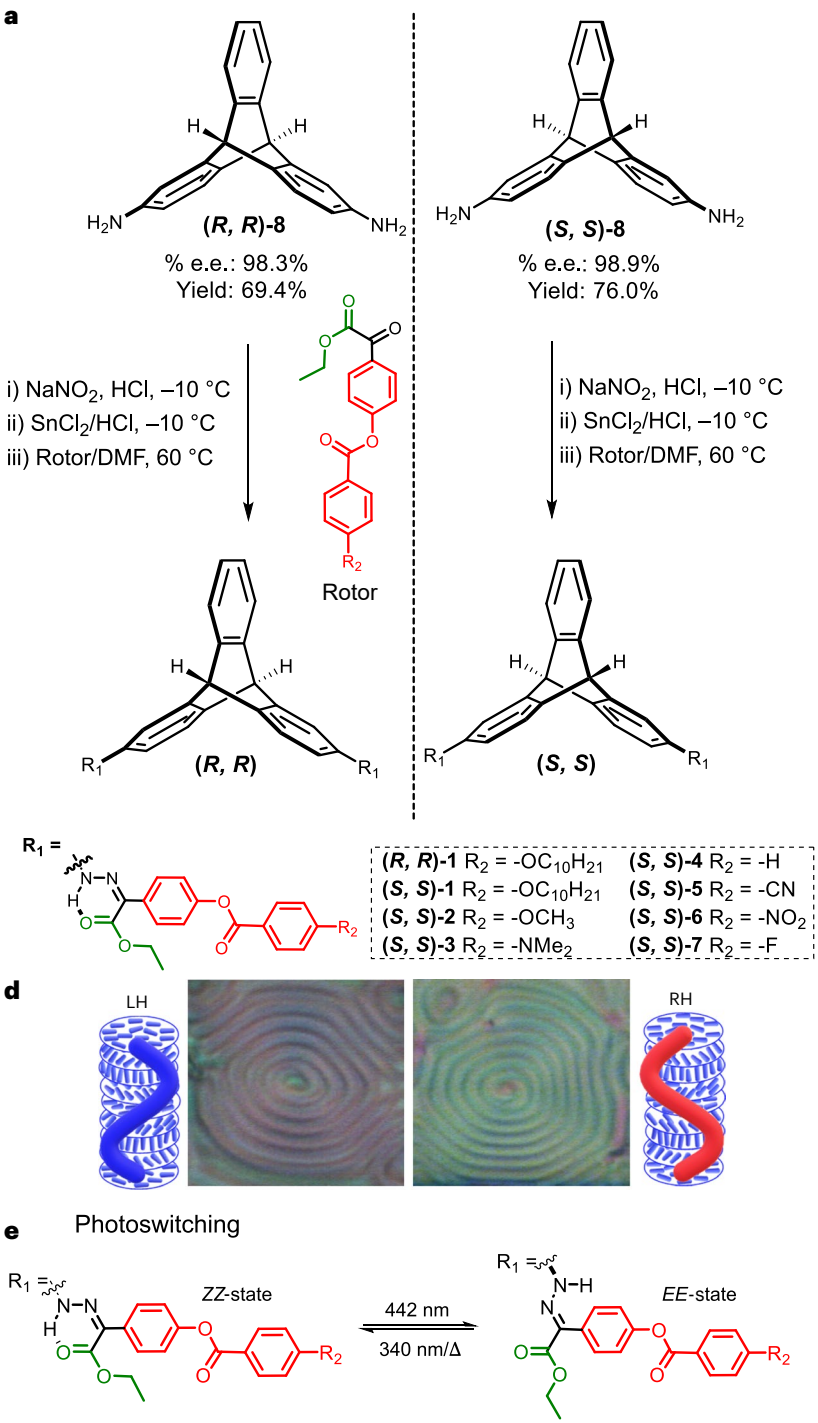

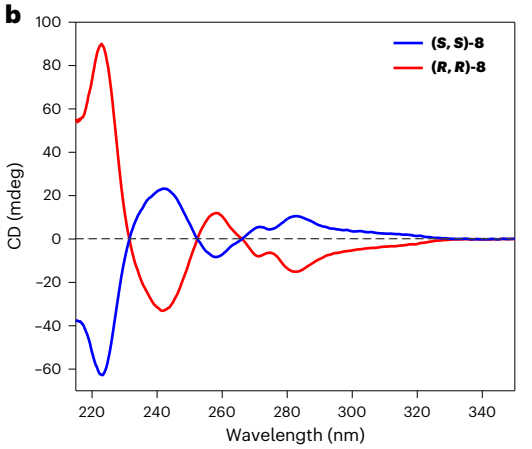

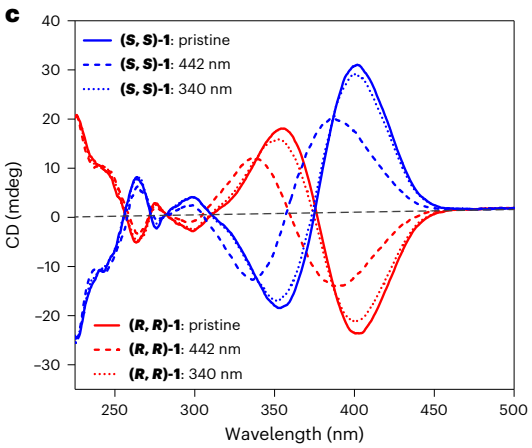

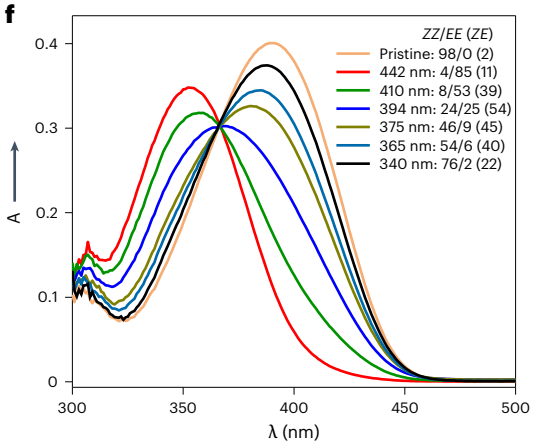

Fig. 1 | Photochromic triptycene chiral dopants, their synthesis, characterization and photoisomerization studies. a, Synthesis of the triptycene-based photochromic chiral dopants (***R***,***R***)-**1**/(***S***,***S***)-**1** to (***S***,***S***)-**7** from the corresponding enantiomers (***R***,***R***)-**8** and (***S***,***S***)-**8**, respectively. **b**,**c**, CD spectra of the triptycene diamines (**b**) and photoswitches (***R***,***R***)-**1** and (***S***,***S***)-**1** in their pristine, PSS_{442} and PSS_{340} states (**c**). **d**, Spiral textures corresponding to (***R***,***R***)-**1** (left-handed (LH)) and (***S***,***S***)-**1** (right-handed (RH)) doped 5CB (0.45 mol%). **e**, The photoisomerization process of the triptycene–hydrazone chiral dopants. The switch toggles mainly between the *ZZ* isomer to predominantly the *EE* upon 442 and 340 nm light irradiation, respectively. **f**, UV–vis spectra of the different PSSs that can be obtained as a function of the applied wavelength. The ratio of the isomers (*ZZ*, *EE* and *ZE*) obtained at each PSS is also indicated. A, absorption.

the photoisomerization resulted in a multi-stage change in the reflection wavelength and triggered a rare isothermal phase transition from cholesteric to chiral smectic phase, enabling the creation of a light-gated optical window. To address the issue of low β and $\Delta\beta$ values, which is a general limitation of isosorbides[35], and to extend the limited structural space of chiral motifs available to practitioners[1,6,7], we decided to develop triptycene[36] as the chiral core of the switchable dopant. Triptycene is not a newcomer to the LC field as triptycene-based LCs that exhibit smectic phases were initially reported by Norvez and co-workers[37,38] while Swager's group discovered that they can also result in nematic phases[39,40]. Our choice of triptycene[41,42] was inspired by the latter's finding that this motif enhances the molecular alignment of LCs and stretched polymers, while increasing the solubility of the latter in LCs[43–46].

Here, we demonstrate how triptycene can be used as the chiral building block of photoswitchable dopants (Fig. 1a) resulting in large β values, thus expanding the toolbox available for practitioners, and how its combination with bistable hydrazones results in tunable, multi-stage and long-lived multi-colour reflections in CLCs. We first studied the effect of the pendent group (R_2 in Fig. 1a) on the β and $\Delta\beta$ values of the dopant. These studies showed that conformational flexibility, dispersion forces and π−π interactions play a crucial role in determining these values. Next, we used the relatively large β (53 μm^{-1} for the *ZZ*-rich state and 107 μm^{-1} for the *EE*-rich state) and $\Delta\beta$ (change in β upon photoisomerization) values (54 μm^{-1}) of the best dopant **(*S*, *S*)-1**, in combination with the unique properties that bistability affords (that is, locking-in of different isomer ratios of the hydrazone and hence different properties in the same material)[34,47], to access various non-equilibrated persistent states (that is, kinetically trapped ones) of the LC self-assembly, as a function of wavelength or irradiation time, resulting in stable reflection of the primary red, green and blue (RGB) colours from the surfaces. With these properties, in combination with an easy to implement digital light processing (DLP) microscope projection set-up[48], we were able to develop reconfigurable and rewritable canvases that display photoreversible and stable multi-colour images. These photoresponsive multi-colour reflective surfaces require no power to maintain their properties and are a promising strategy for the advancement of long-lived, light-driven and light-configurable energy-efficient displays[49], among other applications.

Results and discussion

Molecular design, synthesis and characterization

To synthesize the chiral dopants **(*R*, *R*)-1**/**(*S*, *S*)-1** to **(*S*, *S*)-7** (Fig. 1a), we first prepared the enantiomerically pure diamines **(*R*, *R*)-8** and **(*S*, *S*)-8**. To this end, we synthesized racemic 2,6-diaminotriptycene by nitrating triptycene followed by reduction using a reported procedure (Supplementary Scheme 1)[50]. The racemate was then resolved into its enantiomers (using a CHIRALCEL OD-H column (MeOH + 0.1% Et_2NH) (Supplementary Scheme 1) yielding an enantiomeric excess (% e.e.) of 98.3 and 98.9% for **(*R*, *R*)-8** and **(*S*, *S*)-8**, respectively (Supplementary Fig. 1). The enantiomers were characterized by circular dichroism (CD) spectroscopy, which yielded the expected mirror images (Fig. 1b). The absolute configuration of the enantiomers was assigned by relying on a previous report[51]. With the enantiomers in hand, the target dopants were synthesized in a straightforward manner (Fig. 1a) and characterized by using NMR (intermediates and target dopants; Supplementary Figs. 2–38) spectroscopy and high-resolution spectrometry. The CD spectra for the enantiomeric pair **(*R*, *R*)-1** and **(*S*, *S*)-1** showed excellent mirror images indicating no loss in chirality during the reaction cycle (Fig. 1c). The reason for directly attaching the photoswitchable units to the chiral motif was to amplify the geometrical change upon photoisomerization, while the LC compatible 4-decyloxyphenyl benzoate units in dopant **1** were used to enhance the dopant's solubility in the LC matrix. Our hypothesis was that these structural elements will result in high β and $\Delta\beta$ values. To further test this hypothesis and investigate the effect of the terminal decyl alkoxy chain (-$OC_{10}H_{21}$) on the dopant's properties, we replaced this unit with -OMe, -NMe_2, -H, -CN, -NO_2 and -F groups. The *S* configuration was chosen for these studies because **(*S*, *S*)-1** exhibited a higher $\Delta\beta$ value than **(*R*, *R*)-1**.

Photophysics, helical twisting power (β) and structure–property analysis

The photophysical and photoisomerization (Fig. 1b,c,e,f) properties of the enantiomeric dopants (**1**–**7**) were studied using UV–visible (UV–vis), CD and ^{1}H NMR spectroscopies (Supplementary Figs. 39–87 and Supplementary Tables 1–11). For instance, irradiation of pristine samples of **(*S*, *S*)-1** (λ_{max} = 390 nm, ε = 40,120 M^{-1} cm^{-1}, 98% *ZZ*) in toluene with 442 nm light affords a photostationary state (PSS_{442}) consisting of 85% *EE* (λ_{max} = 354 nm, ε = 36,540 M^{-1} cm^{-1}) and a minor *ZE* population (11%) along with minimal amount of the *ZZ* isomer (4%) (Fig. 1f). Upon irradiation with 340 nm light, the majority *ZZ* state (76%) is restored along with minor fraction of the *ZE* (22%) and negligible amount of *EE* state (2%) (Supplementary Table 2). The quantum yields for the *Z*→*E* isomerization and its reverse process were 1.79 ± 0.05% and 3.26 ± 0.36%, respectively (Supplementary Fig. 81), and the calculated thermal isomerization half-life of the photoswitch was 11 years in toluene and 25 years in the LC phase (Supplementary Tables 9 and 10). The fatigue resistance of the switch was also studied both in solution and the LC phase, and after ten consecutive switching cycles minimal change in absorption intensity was observed for the former (Supplementary Fig. 45) and barely any change was observed after 20 consecutive switching cycles in the latter (Fig. 2c and Supplementary Fig. 92a). We also made use of the bistability of the system to obtain and lock-in different *Z*/*E* isomer ratios (that is, different PSSs) of **(*S*, *S*)-1** as a function of irradiation wavelength (Fig. 1f and Supplementary Table 2). The photophysical and photoisomerization studies were also performed for the other enantiomer **(*R*, *R*)-1** as well as the other chiral dopants **2**–**7**, the details of which can be found in Supplementary Figs. 39–87 and Supplementary Tables 1–8. These switches did not exhibit discernible substituent effects on the absorption wavelengths, PSSs, quantum yields or half-lives, relative to **(*S*, *S*)-1** (Supplementary Tables 9 and 11).

The switching of the dopants was also monitored in solution using CD spectroscopy (Fig. 1c). Initially, dopants **(*R*, *R*)-1** and **(*S*, *S*)-1** display large positive and negative Cotton effects in the region between 300 and 470 nm, corresponding to the absorption band of the pristine *Z* form of the derivatives (Supplementary Fig. 78). Upon irradiation with 442 nm visible light (up to PSS), the strong excitation couplet peaks at 356 and 402 nm decrease in intensity, accompanied by a blue shift because of the photoisomerization of the hydrazone chromophore. Considering the fact that the chiral nature of the triptycene is not affected by the photoswitching units, these spectral changes mirror the ones observed for the dopants in the UV–vis spectra (Supplementary Fig. 78).

To study the effect of the triptycene-based photochromic dopants on the LC properties of achiral nematic hosts, we doped them into the achiral nematic LC 4-cyano-4'-pentylbiphenyl (5CB) resulting in cholesteric phases (Fig. 1d). The dopants showed excellent solubility in the nematic host and induced opposite handedness when doped with enantiomeric pair **(*R*, *R*)-1** and **(*S*, *S*)-1** (Supplementary Fig. 88). The β values of the dopants were measured using the Grandjean–Cano wedge method (Supplementary Fig. 89 and Supplementary Tables 12 and 13)[22,23]. For example, **(*R*, *R*)-1** in 5CB has a β value of −59 μm^{-1} at PSS_{340} (*ZZ*-rich state) which changes to −109 μm^{-1} at PSS_{442} (*EE*-rich state), yielding a relatively large $\Delta\beta$ value of 50 μm^{-1} (Supplementary Fig. 89a).

Similarly, the β values were obtained for **(*S*, *S*)-1** in 5CB as well (+53 μm^{-1} at PSS_{340}, +107 μm^{-1} at PSS_{442} and $\Delta\beta$ = 54 μm^{-1} (Supplementary Fig. 89b). The slight difference in the β values of these dopants most likely results from the subtle variation in their enantiopurity. As can be noted from Table 1, the *E* isomer of these and subsequent dopants have higher β values (that is, better interactions with the LC host) than the *Z* isomer. We attribute this observation to the conformational flexibility of the *E* isomer, which allows it to adopt a structure that interacts better with the host LC versus the more rigid *Z* isomer whose hydrazone core is locked in place because of the intramolecular H bond[34,52]. Exchanging the long decyloxy chain in **1** to a shorter methoxy chain in **2** does not change the β value of the *Z* isomer, whereas the value decreases by 20 μm^{-1} for the *E* isomer. We hypothesize that this change results from the loss of the dispersion interactions between the alkoxy tail and the alkyl chain of 5CB. The β values of **2** (OMe) are similar to **3** (NMe_2), indicating that the electron donating capability of the substituent is not playing a major role in determining these values. Nonetheless, comparing these two dopants with **6** (NO_2) and **7** (F), it becomes evident that π−π interactions between the dopant and LC host are important as well. These interactions are stronger in both

https://doi.org/10.1038/s41557-024-01648-0

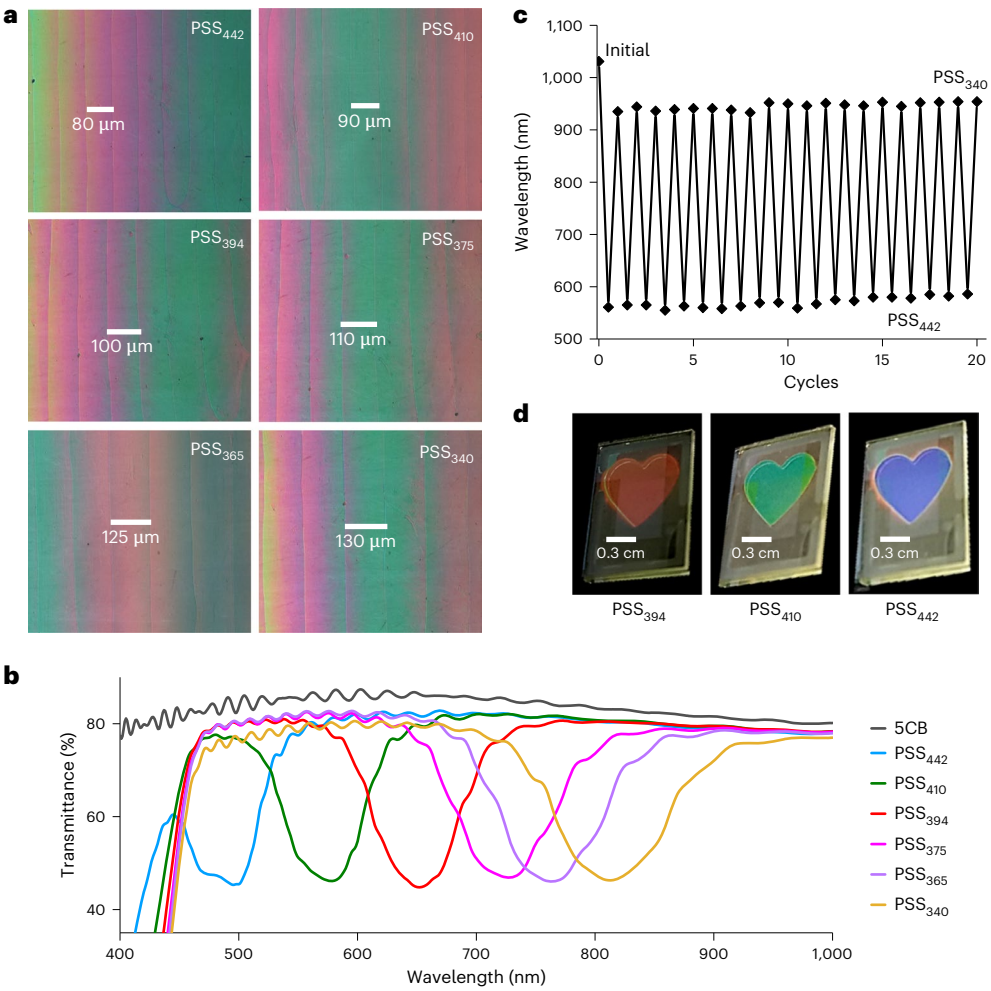

Fig. 2 | Photochemical response and fatigue resistance of 5CB doped (*S*, *S*)-1: polarized optical micrographs, transmittance spectra and RGB images. **a**, Polarized optical micrographs of the (***S***, ***S***)-**1** sample (0.45% in 5CB) in Cano wedge cells after irradiations with 442, 410, 394, 375, 365 and 340 nm light. **b**, The change in the transmittance spectra of 5CB doped (3.1 mol%) with (***S***, ***S***)-**1** as a function of irradiation wavelength. **c**, Fatigue resistance of CLC mixture (5CB doped with (***S***, ***S***)-**1** (2.91 mol%) in a 5-μm-thick planar cell) monitored by following the transmittance bands upon switching from between PSS_{340} and PSS_{442} for 20 times. **d**, Photomicrographs of RGB coloured heart-shaped images obtained by irradiating 5-μm-thick planar cells (with parallel rubbing) of a masked CLC mixture (3.1 mol% doped (***S***, ***S***)-**1** in 5CB).

Table 1 | Helical twisting powers, β (μm^{-1}) in 5CB[a]

Chiral dopants	PSS_{340} (*ZZ*-rich state)	PSS_{442} (*EE*-rich state)	$\Delta\beta$[b]
(***R***, ***R***)-**1**	−59	−109	50
(***S***, ***S***)-**1**	+53	+107	54
(***S***, ***S***)-**2**	+52	+85	33
(***S***, ***S***)-**3**	+49	+87	38
(***S***, ***S***)-**4**	+28	+76	48
(***S***, ***S***)-**5**	+47	+85	38
(***S***, ***S***)-**6**	+31	+55	24
(***S***, ***S***)-**7**	+35	+59	24

[a]β values were calculated using the Grandjean–Cano wedge method with the EHC KCRK07 wedge cell at room temperature (~22 °C). [b]The difference in helical twisting power ($\Delta\beta$) between the PSS_{340} (majority *ZZ* isomer) and PSS_{442} (majority *EE* isomer).

the *E* and *Z* forms of **2** and **3** because they have an electron-rich aromatic core that interacts better with the electron-poor π core of 5CB, whereas the electron-poor cores of **6** and **7** result in weaker interactions. These results also showcase that highly polarizable groups such as F, which induce strong dipole moments, do not always yield large β values[53]

The exception in the electron withdrawing series is dopant **5**, which has a CN group making its π core similar to that of 5CB, allowing it to interact with the LC host as good as **2** and **3** do; that is, the structural similarity is enhancing the interactions between host and guest[54–56]. Finally, the β value of the unsubstituted dopant **4** in the *Z* form is similar to that of **6** and **7**, indicating that these three dopants have adopted the minimal interaction possible in this configuration. Meanwhile, the β value in the *E* form is intermediate between the electron donating and pushing groups, clearly showcasing the importance of conformational flexibility of the dopant in optimizing electron rich/poor and poor/poor π–π interactions in such systems. This observation is very important as it negates a rule of thumb in the field that rigid dopant structures are needed for high β values[3]. Overall, this structure–property analysis sheds light on the molecular-level interactions that govern the mechanism by which chirality transfer occurs from dopant to LC host, which is one of the biggest unknowns in the field[55].

To demonstrate the ability of the dopants to kinetically trap the helical assembly at a particular pitch based on the irradiation wavelength (that is, PSS), samples of the best performing (that is, highest β and $\Delta\beta$; Table 1) dopants (***R***, ***R***)-**1** and (***S***, ***S***)-**1** (Fig. 2a) in 5CB were irradiated with 340, 365, 375, 394, 410 and 442 nm light until the appropriate PSS was reached (that is, when the helical pitch no longer

https://doi.org/10.1038/s41557-024-01648-0

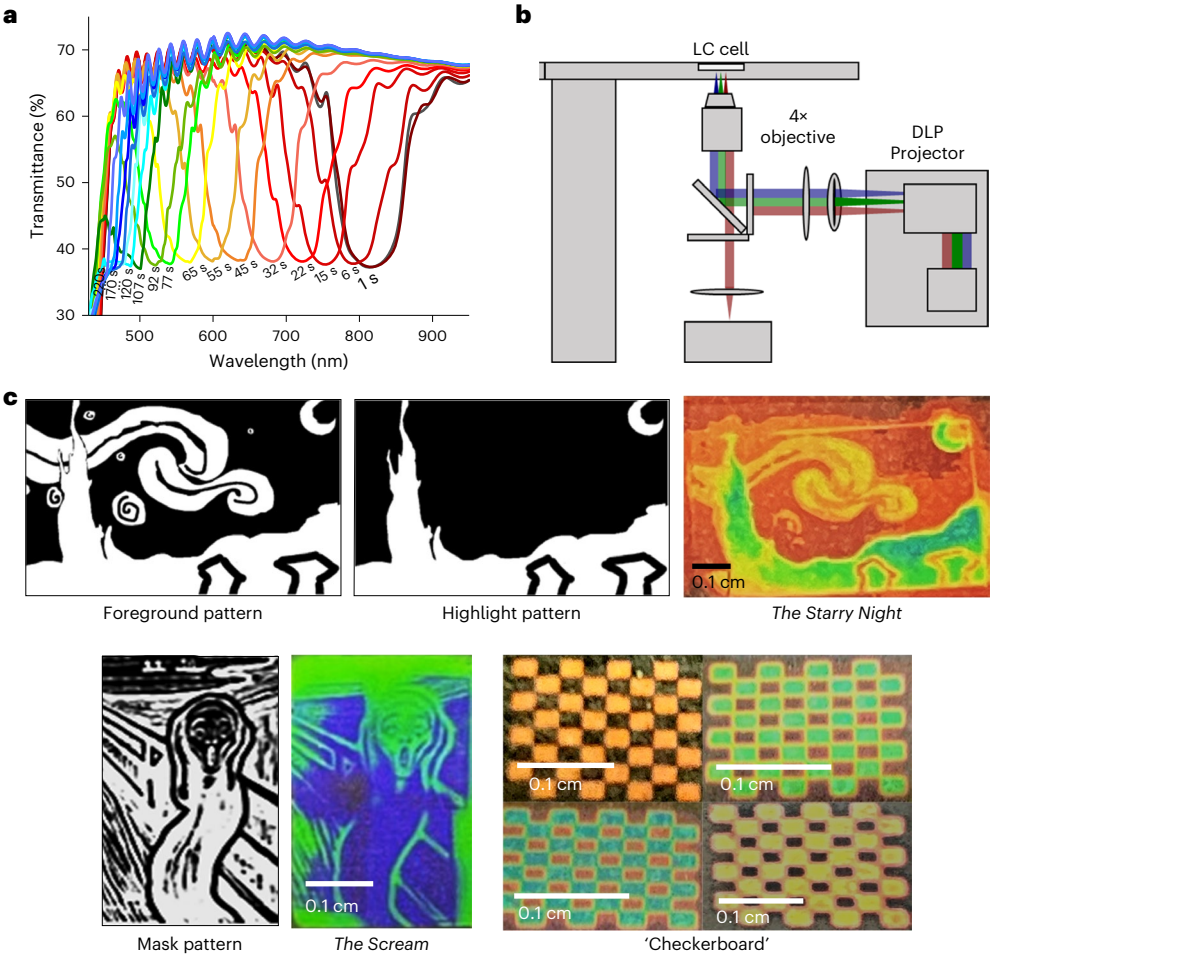

Fig. 3 | Transmittance spectra and DLP patterning of 5CB doped (*S*, *S*)-1 for multi-colour image generation. a, The change in the transmittance spectra of 5CB doped with **(*S*, *S*)-1** as a function of different irradiation times with 442 nm wavelength of light. **b**, A schematic of the DLP patterning set-up used to create multi-colour images by controlling irradiation time on a particular area (reprinted (adapted) from ref. 48 with permission of the American Chemical Society). **c**, Patterns projected and produced for DLP patterning experiments: Van Gogh's *The Starry Night* (Vincent van Gogh, *The Starry Night*, 1889; photo credit: digital image from The Museum of Modern Art/Licensed by SCALA/Art Resource, NY) with foreground pattern (left), highlight pattern (middle) and image produced on the LC cell (right). Bottom: Edvard Munch's *The Scream* (Edvard Munch, *The Scream*, 1893; photo credit: Børre Høstland/The National Museum) and checkerboard images produced on the LC cell. Transmittance spectra and all the DLP patterned multi-coloured images shown here are recorded in 5-µm-thick planar cells (with parallel rubbing) filled with the CLC mixture (3.2 mol% of **(*S*, *S*)-1** in 5CB). Panel **b** adapted with permission from ref. 48, American Chemical Society. Credit: **c**, digital image of *The Starry Night*, The Museum of Modern Art/Licensed by SCALA/Art Resource; photograph of *The Scream*, Børre Høstland/The National Museum.

changed with continued irradiation). The wavelength-dependent *P* values are summarized in Supplementary Table 14. In general, the *P* length becomes longer when using shorter irradiation wavelengths. Importantly, the thermal stability of the hydrazone switch allowed us to lock in the different pitches of the LC as a function of their different wavelength-dependent PSSs for extended periods of time. We also demonstrated that different pitches can be obtained and locked it as a function of the irradiation time at a given wavelength (for example, 442 nm (vide infra)). It is worth bearing in mind that the LC system is a supramolecular self-assembled helical superstructure, and what we are accomplishing here is the kinetic (that is, out-of-equilibrium) trapping of these different self-assemblies as a function of irradiation wavelength or time.

Adaptive reflective films and DLP

To take advantage of the kinetic trapping property and the relatively large β and $\Delta\beta$ of the dopants, we made adaptive reflective films by loading doped 5CB into planarly aligned LC cells (5 µm cell thickness). The transmittance data obtained from these films, which were measured as a function of irradiation wavelength (Fig. 2b for **(*S*, *S*)-1**) or irradiation times (Fig. 3a and Supplementary Fig. 90 for **(*S*, *S*)-1**) show excellent control over the reflection colour from the visible to the NIR region (for example, from 485 to 812 nm when scanning the wavelength from 442 to 340 nm, respectively). Importantly, the thermal stability of the hydrazones allowed us to lock-in all these states and associated reflected colours for extended periods of time (up to 9 days; Supplementary Fig. 91). To showcase the abilities of the dopant, we engineered a system such that it can reflect the primary colours, RGB, at PSS_{394}, PSS_{410} and PSS_{442}, respectively (Fig. 2d), and then used masks to draw and then redraw (after erasing) RGB coloured heart-shaped patterns using the same LC films. These canvases exhibit remarkable efficiency in repeatedly creating and erasing patterns, attributed to the excellent fatigue resistance of the chiral switch (Supplementary Fig. 92). As for dopants **2**–**7**, their β and $\Delta\beta$ values are moderate enough to enable the fine adjustment of light reflectance even in the visible region (Supplementary Figs. 93–97).

Considering that we have a unique way of controlling the reflected colours and their stability, we decided to use the LC films as canvases on which we can draw more complex multi-colour images, which can be erased and rewritten on demand. Using a DLP microscope projection (Fig. 3b)[48], we patterned multi-colour images (Fig. 3c), with a resolution

of 76 µm (Supplementary Fig. 99) by controlling illumination times of patterned blue light-emitting diode light centred at 450 nm. For dual-colour images, the desired images were deconstructed using GNU Image Manipulation Program (GIMP 2.10.30) into a processed image for patterning a blue foreground with a green background using 16 s illumination time (Supplementary Fig. 98a and Supplementary Table 15). Following this procedure, a single-colour images of 'Checkerboard' and a dual-colour image of Edvard Munch's *The Scream* was printed onto the LC canvas. Inclusion of more colours was readily achieved by deconstructing the image into two patterns for a 'foreground' and 'highlight' by illuminating the 'foreground' pattern for 4 s, illuminating the 'highlight' pattern for 4–12 s and leaving an unpatterned background for the third colour. This procedure was used to generate unprecedented CLC multi-colour images including Van Gogh's *The Starry Night* in the same cell after write/erase cycles.

Conclusions

Here, we demonstrate the use of triptycene as the chiral element of a photoswitchable dopant. The fact that this scaffold results in a large β value drastically expands the chiral unit toolbox available for practitioners, which has so far mainly focused on binaphthyl derivatives[6,7]. The combination of triptycene with the large geometrical change that hydrazones undergo upon photoisomerization results in large $\Delta\beta$ values. The structure–property analysis yielded much-needed insights about the molecular-level mechanisms that control the chirality transfer between the dopant and host LC. This information will be of utmost importance to practitioners who are interested in designing efficient chiral dopants. Finally, the $\Delta\beta$ of dopant **1** allowed for the modulation of the LC reflected light from the visible to the NIR range (450–800 nm, when changing irradiation time). Meanwhile, the bistability of the hydrazone enabled the long-term locking-in of the reflected colour as a function of wavelength, yielding a surface that can be patterned to reflect the primary RGB colours. The same property also allowed us to use the irradiation time of visible light (442 nm) to lock-in different colours, which when combined with a simple DLP microscope projection set-up, produces multi-colour pictures. Future work will focus on enhancing the β and $\Delta\beta$ values of the dopants, which are currently not as large as those measured in azobenzene (with the caveat being that the latter result in an isotropic LC upon switching). Additionally, we will explore the use of the dopants in triptycene-based LCs[37–40] to take advantage of the structural similarities between them that, as observed with dopant **4**, should result in an improved chirality transfer and, hence, β values. Finally, we plan to investigate the application of these dopants in active smart surfaces, sensors, nonlinear optical materials and colour filters[7,57,58].

Online content

Any methods, additional references, Nature Portfolio reporting summaries, source data, extended data, supplementary information, acknowledgements, peer review information; details of author contributions and competing interests; and statements of data and code availability are available at https://doi.org/10.1038/s41557-024-01648-0.

References

1. Li, Q. *Intelligent Stimuli-Responsive Materials: from Well-Defined Nanostructures to Applications* (Wiley, 2013).
2. Goulet-Hanssens, A., Eisenreich, F. & Hecht, S. Enlightening materials with photoswitches. *Adv. Mater.* **32**, 1905966 (2020).
3. Wang, Y. & Li, Q. Light-driven chiral molecular switches or motors in liquid crystals. *Adv. Mater.* **24**, 1926–1945 (2012).
4. Kim, Y. & Tamaoki, N. Photoresponsive chiral dopants: light-driven helicity manipulation in cholesteric liquid crystals for optical and mechanical functions. *ChemPhotoChem.* **3**, 284–303 (2019).
5. Zheng, Z. et al.Three-dimensional control of the helical axis of a chiral nematic liquid crystal by light. *Nature* **531**, 352–356 (2016).
6. Bisoyi, H. K. & Li, Q. Light-driven liquid crystalline materials: from photo-induced phase transitions and property modulations to applications. *Chem. Rev.* **116**, 15089–15166 (2016).
7. Bisoyi, H. K. & Li, Q. Liquid crystals: versatile self-organized smart soft materials. *Chem. Rev.* **122**, 4887–4926 (2021).
8. Broer, D. J., Lub, J. & Mol, G. N. Wide-band reflective polarizers from cholesteric polymer networks with a pitch gradient. *Nature* **378**, 467–469 (1995).
9. Chilaya, G. S. Light-controlled change in the helical pitch and broadband tunable cholesteric liquid-crystal lasers. *Crystallogr. Rep.* **51**, S108–S118 (2006).
10. Palffy-Muhoray, P. Liquid crystals new designs in cholesteric colour. *Nature* **391**, 745–746 (1998).
11. Sagisaka, T. & Yokoyama, Y. Reversible control of the pitch of cholesteric liquid crystals by photochromism of chiral fulgide derivatives. *Bull. Chem. Soc. Jpn* **73**, 191–196 (2000).
12. Janicki, S. Z. & Schuster, G. B. A liquid crystal opto-optical switch: nondestructive information retrieval based on a photochromic fulgide as trigger. *J. Am. Chem. Soc.* **117**, 8524–8527 (1995).
13. White, T. J. et al. Optically reconfigurable color change in chiral nematic liquid crystals based on indolylfulgide chiral dopants. *J. Mater. Chem.* **22**, 5751–5757 (2012).
14. Kurosaki, Y., Sagisaka, T., Matsushima, T., Ubukata, T. & Yokoyama, Y. Chiral, thermally irreversible and quasi-stealth photochromic dopant to control selective reflection wavelength of cholesteric liquid crystal. *ChemPhysChem* **21**, 1375–1383 (2020).
15. Bosco, A. et al. Photoinduced reorganization of motor-doped chiral liquid crystals: bridging molecular isomerization and texture rotation. *J. Am. Chem. Soc.* **130**, 14615–14624 (2008).
16. Koumura, N., Zijlstra, R. W., van Delden, R. A., Harada, N. & Feringa, B. L. Light-driven monodirectional molecular rotor. *Nature* **401**, 152–155 (1999).
17. van Delden, R. A., Koumura, N., Harada, N. & Feringa, B. L. Unidirectional rotary motion in a liquid crystalline environment: color tuning by a molecular motor. *Proc. Natl Acad. Sci. USA* **99**, 4945–4949 (2002).
18. Ryabchun, A. et al. Helix inversion controlled by molecular motors in multistate liquid crystals. *Adv. Mater.* **32**, 2004420 (2020).
19. Hou, J. et al. Photo-responsive helical motion by light-driven molecular motors in a liquid-crystal network. *Angew. Chem. Int. Ed.* **60**, 8251–8257 (2021).
20. Bandara, H. D. & Burdette, S. C. Photoisomerization in different classes of azobenzene. *Chem. Soc. Rev.* **41**, 1809–1825 (2012).
21. Irie, M., Fukaminato, T., Matsuda, K. & Kobatake, S. Photochromism of diarylethene molecules and crystals: memories, switches, and actuators. *Chem. Rev.* **114**, 12174–12277 (2014).
22. Li, Y., Urbas, A. & Li, Q. Reversible light-directed red, green, and blue reflection with thermal stability enabled by a self-organized helical superstructure. *J. Am. Chem. Soc.* **134**, 9573–9576 (2012).
23. Li, Y., Xue, C., Wang, M., Urbas, A. & Li, Q. Photodynamic chiral molecular switches with thermal stability: from reflection wavelength tuning to handedness inversion of self-organized helical superstructures. *Angew. Chem. Int. Ed.* **52**, 13703–13707 (2013).
24. Li, Y., Wang, M., Wang, H., Urbas, A. & Li, Q. Rationally designed axially chiral diarylethene switches with high helical twisting power. *Chem. Eur. J.* **20**, 16286–16292 (2014).
25. Denekamp, C. & Feringa, B. L. Optically active diarylethenes for multimode photoswitching between liquid–crystalline phases. *Adv. Mater.* **10**, 1080–1082 (1998).
26. Uchida, K., Kawai, Y., Shimizu, Y., Vill, V. & Irie, M. An optically active diarylethene having cholesterol units: a dopant for photoswitching of liquid crystal phases. *Chem. Lett.* **29**, 654–655 (2000).

27. Yamaguchi, T., Inagawa, T., Nakazumi, H., Irie, S. & Irie, M. Photoswitching of helical twisting power of a chiral diarylethene dopant: pitch change in a chiral nematic liquid crystal. *Chem. Mater.* **12**, 869–871 (2000).
28. van Leeuwen, T. et al. Photoinduced pitch changes in chiral nematic liquid crystals formed by doping with chiral diarylethene. *J. Mater. Chem.* **21**, 3142–3246 (2011).
29. Li, Y., Urbas, A. & Li, Q. Synthesis and characterization of light-driven dithienylcyclopentene switches with axial chirality. *J. Org. Chem.* **76**, 7148–7156 (2011).
30. Zheng, Z. et al. Digital photoprogramming of liquid-crystal superstructures featuring intrinsic chiral photoswitches. *Nat. Photonics* **16**, 226–234 (2022).
31. Shao, B. & Aprahamian, I. Hydrazones as new molecular tools. *Chem* **6**, 2162–2173 (2020).
32. Qian, H., Pramanik, S. & Aprahamian, I. Photochromic hydrazone switches with extremely long thermal half-lives. *J. Am. Chem. Soc.* **139**, 9140–9143 (2017).
33. Shao, B., Qian, H., Li, Q. & Aprahamian, I. Structure property analysis of the solution and solid-state properties of bistable photochromic hydrazones. *J. Am. Chem. Soc.* **141**, 8364–8371 (2019).
34. Moran, M. J., Magrini, M., Walba, D. M. & Aprahamian, I. Driving a liquid crystal phase transition using a photochromic hydrazone. *J. Am. Chem. Soc.* **140**, 13623–13627 (2018).
35. Shin, S. et al. Tuning helical twisting power of isosorbide-based chiral dopants by chemical modifications. *Mol. Cryst. Liq. Cryst.* **534**, 19–31 (2011).
36. Khan, M. N. & Wirth, T. Chiral triptycenes: concepts, progress and prospects. *Chem. Eur. J.* **27**, 7059–7068 (2021).
37. Norvez, S. Liquid crystalline triptycene derivatives. *J. Org. Chem.* **58**, 2414–2418 (1993).
38. Norvez, S. & Simon, J. Epitaxygens: mesomorphic properties of triptycene derivatives. *Liq. Cryst.* **14**, 1389–1395 (1993).
39. Long, T. M. & Swager, T. M. Triptycene-containing bis(phenylethynyl)benzene nematic liquid crystals. *J. Mater. Chem.* **12**, 3407–3412 (2002).
40. Lohr, A. & Swager, T. M. Stabilization of the nematic mesophase by a homogeneously dissolved conjugated polymer. *J. Mater. Chem.* **20**, 8107–8111 (2010).
41. Kelly, T. R., Silva, R. A., De Silva, H., Jasmin, S. & Zhao, Y. A rationally designed prototype of a molecular motor. *J. Am. Chem. Soc.* **122**, 6935–6949 (2000).
42. Ube, H., Yasuda, Y., Sato, H. & Shionoya, M. Metal-centred azaphosphatriptycene gear with a photo-and thermally driven mechanical switching function based on coordination isomerism. *Nat. Commun.* **8**, 4296 (2017).
43. Long, T. M. & Swager, T. M. Minimization of free volume: alignment of triptycenes in liquid crystals and stretched polymers. *Adv. Mater.* **13**, 601–604 (2001).
44. Long, T. M. & Swager, T. M. Using 'internal free volume' to increase chromophore alignment. *J. Am. Chem. Soc.* **124**, 3826–3827 (2002).
45. Zhu, Z. & Swager, T. M. Conjugated polymer liquid crystal solutions: control of conformation and alignment. *J. Am. Chem. Soc.* **124**, 9670–9671 (2002).
46. Ohira, A. & Swager, T. M. Ordering of poly(*p*-phenylene ethynylene)s in liquid crystals. *Macromolecules* **40**, 19–25 (2007).
47. Yang, S. et al. Multistage reversible T_g photomodulation and hardening of hydrazone-containing polymers. *J. Am. Chem. Soc.* **143**, 16348–16353 (2021).
48. Haris, U., Plank, J. T., Li, B., Page, Z. A. & Lippert, A. R. Visible light chemical micropatterning using a digital light processing fluorescence microscope. *ACS Cent. Sci.* **8**, 67–76 (2021).
49. Gu, C., Jia, A.-B., Zhang, Y.-M. & Zhang, S. X.-A. Emerging electrochromic materials and devices for future displays. *Chem. Rev.* **122**, 14679–14721 (2022).
50. Chen, Z. & Swager, T. M. Synthesis and characterization of poly (2,6-triptycene). *Macromolecules* **41**, 6880–6885 (2008).
51. Zhang, Q. P. et al. Triptycene-based chiral porous polyimides for enantioselective membrane separation. *Angew. Chem. Int. Ed.* **133**, 12891–12895 (2021).
52. Ryabchun, A., Li, Q., Lancia, F., Aprahamian, I. & Katsonis, N. Shape-persistent actuators from hydrazone photoswitches. *J. Am. Chem. Soc.* **141**, 1196–1200 (2019).
53. Narazaki, Y., Nishikawa, H., Higuchi, H., Okumura, Y. & Kikuchi, H. Substituent effects of bridged binaphthyl-type chiral dopants on the helical twisting power in dopant-induced chiral liquid crystals. *RSC Adv.* **8**, 971–979 (2018).
54. Eelkema, R. & Feringa, B. L. Amplification of chirality in liquid crystals. *Org. Biomol. Chem.* **4**, 3729–3745 (2006).
55. Pieraccini, S., Masiero, S., Ferrarini, A. & Spada, G. P. Chirality transfer across length-scales in nematic liquid crystals: fundamentals and applications. *Chem. Soc. Rev.* **40**, 258–271 (2011).
56. Katsonis, N., Lacaze, E. & Ferrarini, A. Controlling chirality with helix inversion in cholesteric liquid crystals. *J. Mater. Chem.* **22**, 7088–7097 (2012).
57. Wang, D., Park, S.-Y. & Kang, I.-K. Liquid crystals: emerging materials for use in real-time detection applications. *J. Mater. Chem. C* **3**, 9038–9047 (2015).
58. White, T. J., McConney, M. E. & Bunning, T. J. Dynamic color in stimuli-responsive cholesteric liquid crystals. *J. Mater. Chem. C* **20**, 9832–9847 (2010).

Methods

General

All reagents and starting materials were obtained from commercial sources and used without further purification. All reactions were done under normal atmosphere unless otherwise noted. Compounds were purified by column chromatography using silica gel (SiliCycle, 60 Å, 230–400 mesh) as the stationary phase and eluting solvents are reported as ratios unless otherwise noted. Racemic 2,6-diaminotriptycene was resolved into its (***R***,***R***) and (***S***,***S***) enantiomers by chiral-phase HPLC using a CHIRALCEL OD-H column (MeOH + 0.1% Et_2NH) with enantiomeric excess (% e.e.) of 98.3% (yield 69.4%) and 98.9% (yield 76.0%), respectively. Recrystallizations were performed with HPLC-grade solvents. Deuterated solvents were obtained from Cambridge Isotope Labs and used without further purification. The ^{1}H and ^{13}C NMR spectra were recorded on 500 or 600 MHz instruments with working frequencies of 500.13 and 600.13 MHz for ^{1}H nuclei and 125.8 or 150.9 MHz for ^{13}C nuclei, respectively. Chemical shifts are quoted in parts per million relative to tetramethylsilane, using the residual solvent peak as the reference standard. Electrospray ionization mass spectra were obtained on a Shimadzu LCMS-8030 mass spectrometer. UV–vis and transmittance spectra were recorded on a Shimadzu UV-1800 UV–vis spectrophotometer. Irradiation experiments were conducted with a stand-alone xenon arc lamp system (model LB-LS/30, Sutter Instrument), outfitted with a SMART SHUTTER controller (model LB10-B/IQ, Sutter Instrument) and a liquid light guide LLG/250. In the irradiation experiments, 340 (340HC10- 25), 365 (365HC10-25), 375 (375HC10-25), 394 (394HC10-25) and 410 (410FS10-25) nm light filters, purchased from Andover Corporation, were used. The photon flux for the different wavelengths of light used in all the photoswitching experiments as measured by the chemical actinometery method[33] were as follows: 442 nm: 7.35 × 1,016 photons s^{-1}; 410 nm: 7.17 × 1,016 photons s^{-1}; 394 nm: 8.49 × 1,016 photons s^{-1}; 375 nm: 6.56 × 1,016 photons s^{-1}; 365 nm: 7.83 × 1,016 photons s^{-1} and 340 nm: 9.75 × 1,016 photons s^{-1}. CD spectra were recorded in 1-mm-pathlength quartz cuvette using a JASCO J-815 CD spectrometer equipped with a Peltier thermostat.

LC systems

The LC nematic host 5CB was purchased from Tokyo Chemical Industry (TCI). Doped LC samples were prepared using accurately weighed samples (using an analytical balance) of the chiral dopant and 5CB nematic host. The CLC mixtures were made by dissolving both components in a few drops of spectroscopic-grade dichloromethane, followed by the overnight evaporation of the solvent under high vacuum to ensure that no traces of the solvent is left in the CLC mixtures. The textures of the LC samples were observed using an Olympus BX53 polarized optical microscope, and the photomicrographs were captured using an INSTEC MITO2-MC camera. The planar LC cells (LC3-5.0) were purchased from INSTEC, and the KCRK07 (θ = 0.0183) wedge cells were purchased from EHC Japan. For photopatterning experiments, a heart-shaped black flexible plastic mask was placed on top of the planar LC cell and irradiated with specific wavelengths of light.

The DLP microscope consists of a LightCrafter 4500 projector with the native projection optics removed. Light from an RGB light-emitting diode light engine is reflected off a digital micromirror device chip inside the projector and directed through a 50 mm or 100 mm collimation lens into a cage cube mounted with a 90:10 beam splitter. The beam splitter directs the collimated patterned light through a 4× microscope objective to focus onto the LC cell (Fig. 3b). Adjusting the focal length of the collimation lens allows for easy manipulation of image size and we were able to achieve a resolution of 76 µm line widths using a 100 mm lens. For the DLP experiments, LC cells were placed on top of a microscope slide and mounted on the DLP microscope. To expand the area of the projection and to fill the cell, a 50 mm achromatic doublet was used as a collimating lens as opposed to the previously described 100 mm lens[49]. The projected image was focused and aligned using weak red light (0.022 W cm^{-2}, 5% pulse width modulation (PWM)), while patterning was performed with strong blue light (0.475 W cm^{-2}, 100% PWM), with colour variation achieved via varying exposure time as opposed to intensity. Exposure times are noted in Supplementary Table 15, with the images projected in reported in Supplementary Fig. 98. For the resolution determination via microscopic patterning (Supplementary Fig. 99), freshly prepared cells of 5CB doped with (*S*, *S*)-1 at 3.0 mol% were focused on the DLP microscope fitted with a 4× objective and 100 mm collimating lens. Bars of width 48 µm, as measured against a target rheticle (ThorLabs NBS 1952 resolution test target, 3″ × 1″), were projected onto the cell at maximal blue light intensity (0.475 W cm^{-2}) for a 10 s exposure time. Said patterns were imaged on an upright microscope (Zeiss Primovert, 415510-1100-000) via phone camera (Samsung Galaxy S23 Ultra), and the minimum line width resolvable was measured via analysis in ImageJ as 76.07 µm ± 24.17% (n = 72).

Data availability

The data that support the findings of this study are available within the Article and its Supplementary Information. Source data are provided with this paper.

Acknowledgements

I.A. is thankful for the generous support from National Science Foundation (NSF) Division of Materials Research (DMR) (2104464). A.R.L. gratefully acknowledges support from the Welch Research Foundation (N-2038-202004010). We thank L.D. Custis for experimental support. I.A. is thankful to T. Swager (Massachusetts Institute of Technology) for suggesting the use of triptycene as the chiral motif in LC dopants at a Telluride workshop in 2016, and T. Ikai (Nagoya University) for supplying racemic 2,6-diaminotriptycene at a very early stage of this research.

Author contributions

I.B., J.T.P., D.H. and B.B. planned and carried out the experimental work and characterization studies. I.A. and A.R.L. directed the research. All authors contributed to the analysis of the results and the writing of the manuscript.

Competing interests

A.R.L. declares a financial stake in BioLum Sciences, LLC. The remaining authors declare no competing interests.

Additional information

Supplementary information The online version contains supplementary material available at https://doi.org/10.1038/s41557-024-01648-0.

Correspondence and requests for materials should be addressed to Ivan Aprahamian.

Peer review information *Nature Chemistry* thanks Masoud Kazem-Rostami, Quan Li and the other, anonymous, reviewers for their contribution to the peer review of this work.